Hidden order in quantum many-body dynamics of driven-dissipative nonlinear photonic lattices

Jirawat Tangpanitanon,[1,*] Stephen R. Clark,[2,3] V. M. Bastidas,[4] Rosario Fazio,[5,6]
Dieter Jaksch,[7,1] and Dimitris G. Angelakis[1,8,†]

[1]*Centre for Quantum Technologies, National University of Singapore, 3 Science Drive 2, Singapore 117543*
[2]*Department of Physics, University of Bath, Claverton Down, Bath BA2 7AY, United Kingdom*
[3]*Max Planck Institute for the Structure and Dynamics of Matter, CFEL, Hamburg, Germany*
[4]*NTT Basic Research Laboratories & Research Center for Theoretical Quantum Physics, 3-1 Morinosato-Wakamiya, Atsugi, Kanagawa, 243-0198, Japan*
[5]*Abdus Salam ICTP, Strada Costiera 11, I-34151 Trieste, Italy*
[6]*NEST, Scuola Normale Superiore and Istituto Nanoscienze-CNR, I-56126 Pisa, Italy*
[7]*Clarendon Laboratory, University of Oxford, Parks Road, Oxford OX1 3PU, United Kingdom*
[8]*School of Electrical and Computer Engineering, Technical University of Crete, Chania, Greece 73100*

(Received 3 December 2018; published 9 April 2019)

We study the dynamics of nonlinear photonic lattices driven by two-photon parametric processes. By means of matrix-product-state–based calculations, we show that a quantum many-body state with long-range hidden order can be generated from the vacuum. Although this order resembles that characterizing the Haldane insulator, our system is far from equilibrium due to the drive and photon loss. A possible explanation highlighting the role of the symmetry of the drive and the effect of photon loss is discussed. An implementation based on superconducting circuits is proposed and analyzed.

DOI: 10.1103/PhysRevA.99.043808

I. INTRODUCTION

Advances in quantum optics over the past decades have made it possible to engineer strong interactions between individual photons [1]. This motivates its use for generating new kinds of strongly correlated states of light and matter [2,3] for quantum simulation [4,5]. Indeed, early theoretical works have shown that arrays of coupled nonlinear cavities can exhibit a Mott insulator to superfluid phase transition of light, if dissipation is negligible [6–8]. Subsequent works have also shown the possibility to realize a family of many-body phenomena with photons, including effective spin models [9], the fractional quantum Hall effect [10], and topologically protected transport of quantum states [11]. Moreover, the signatures of localization of interacting photons in a quasiperiodic potential have recently been observed with a nine-site superconducting circuit [12].

Interacting photons provide a natural setting for simulating open quantum systems because photons dissipate to the environment and because they can be coherently driven. The coupling to the environment is usually assumed to be weak and the bath is memoryless, in which case the system could reach a dynamically stable steady state that depends on the symmetries of the system [13,14]. Early theoretical works have shown that such steady states manifest various quantum many-body phases [15–22] and can exhibit a dissipative phase transition (DPT) [23,24]. A nonlinear superconducting circuit with up to 72 sites has also been fabricated to study DPTs [21].

Following the success of Landau's symmetry-breaking theory in describing classical and ground-state phases of matter, local order parameters have also been used to classify these new nonequilibrium steady-state phases [14–19,21,23,24]. However, in equilibrium systems, there are phases that do not follow Landau's symmetry-breaking theory [25]. The latter can be probed, for example, by nonlocal order parameters [26,27] or the existence of edge states [28,29]. These phases are symmetry-protected topological (SPT) phases [30,31] and phases with topological order [32,33]. Experimental realizations of topological phases have been explored in various quantum technology platforms, including cold atoms [34] and photonic systems [35,36].

In this work, we study the role of a nonlocal order parameter in the driven-dissipative dynamics of a quantum many-body system and its connection to the underlying symmetry. Specifically, we consider a nonlocal hidden order, analogous to the famous SPT phase characterizing the equilibrium Haldane insulator (HI) phase [37–39]. The system we consider is a lossy nonlinear photonic lattice of the extended Bose–Hubbard type [37–39] which in the right regime can be mapped to the spin-1 Haldane model [40,41] and driven by a two-photon parametric process [18,42,43]. By using matrix-product-state–based calculations [44,45], we show that this process drives the vacuum into a quantum many-body state with nonzero hidden order. We argue that this effect is due to the symmetry of the parametric drive, which cannot be achieved by a conventional one-photon coherent drive. However, the hidden order only remains nonzero for a finite

*a0122902@u.nus.edu
†dimitris.angelakis@qubit.org

time and eventually fades away at the steady state. Instead, we observe a weak density-wave order at the steady state. We analyze this symmetry analytically and numerically by showing that the parametric drive respects the symmetry of the HI state. The natural photon loss breaks the symmetry and therefore plays a negative role in maintaining the hidden order in the dynamics.

This paper is organized as follows: We describe our system including the definition of the hidden order in Sec. II. The symmetry of the parametric process is analyzed in Sec. III. Numerical simulations of the driven-dissipative dynamics showing the evolution of the hidden order are shown and discussed in Sec. IV. In Sec. V, we discuss a conventional one-photon coherent drive which breaks the symmetry of the Haldane phase. We conclude in Sec. VI.

II. THE SYSTEM

We consider a one-dimensional (1D) coupled nonlinear resonator array described by the Hamiltonian $\hat{H}_{\rm tot}^{\rm Lab} = \hat{H}_0 + \hat{H}_{\rm drv}^{\rm par}$, where $\hat{H}_0$ is the extended Bose–Hubbard (EBH) model ($\hbar = 1$),

$$\hat{H}_0 = \omega_r \sum_{i=1}^{L} \hat{n}_i - J \sum_{i=1}^{L-1} (\hat{a}_i^\dagger \hat{a}_{i+1} + \text{H.c.}) + \frac{U}{2} \sum_{i=1}^{L} \hat{n}_i(\hat{n}_i - 1) + V \sum_{i=1}^{L-1} \hat{n}_i \hat{n}_{i+1}, \tag{1}$$

where ω_r is the frequency of the resonator, J is the hopping strength, U is the on-site Kerr nonlinearity, V is the cross-Kerr nonlinearity, and L is the number of sites; see Fig. 1(a). The operator $\hat{a}_i$ is a bosonic annihilation operator at site i and $\hat{n}_i = \hat{a}_i^\dagger \hat{a}_i$ is a local number operator, respectively. The bosonic operators obey the commutation relation $[\hat{a}_i, \hat{a}_j^\dagger] = \delta_{i,j}$ and $[\hat{a}_i, \hat{a}_j] = 0$. Throughout the paper we consider the regime $U \gg J$, which allows us to map the bosonic system onto a spin-1 chain as detailed below. The system is subjected to two-photon nearest-neighbor parametric driving [18,42,43]

$$\hat{H}_{\rm drv}^{\rm par} = \Omega \sum_{i=1}^{L-1} (\hat{a}_i \hat{a}_{i+1} e^{2i\omega_d t} + \text{H.c.}), \tag{2}$$

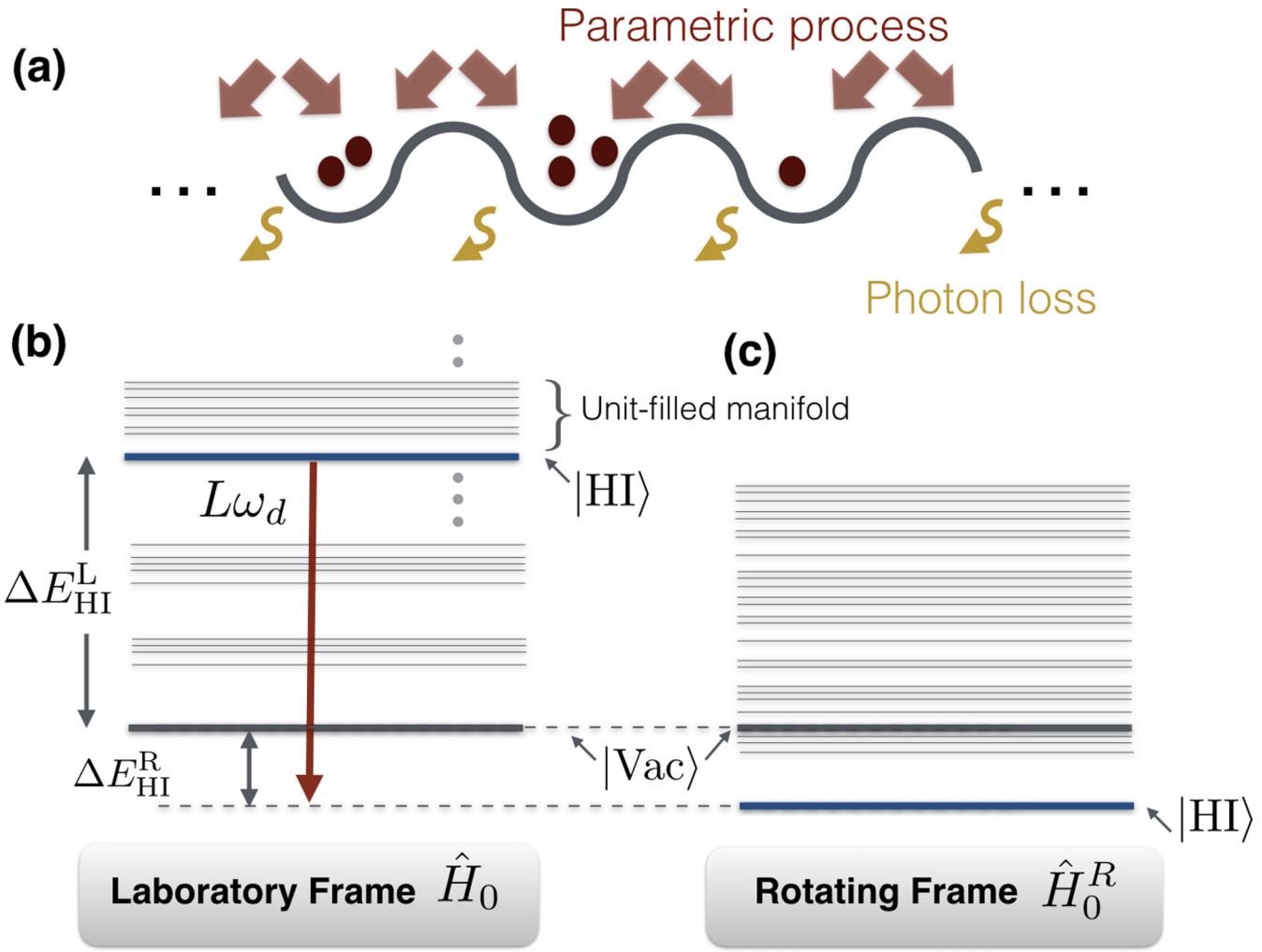

FIG. 1. (a) Sketch of the one-dimensional lossy photonic lattice described by the EBH model and driven by parametric drive. The lower panels show energy spectra of the undriven Hamiltonian in Eq. (1). (b) The laboratory frame and (c) the rotating frame. The red arrow indicates the energy shift $L\omega_d$ of the HI state due to the rotating frame. Since the HI state is a unit-filled state, its energy will be lowered by $L\omega_d$.

where ω_d is the driving frequency and Ω is the amplitude of the drive. A detailed discussion on circuit-QED implementations of this Hamiltonian including parametric drives is presented in Appendix B. We remove the time dependence of the drive by going to the rotating frame defined by $\hat{R} = \exp(i\omega_d t \sum_{i=1}^{L} \hat{n}_i)$. The new Hamiltonian is

$$\hat{H}^{\mathrm{R}}_{\mathrm{tot}} = \hat{R}\hat{H}^{\mathrm{Lab}}_{\mathrm{tot}}\hat{R}^{\dagger} - i\hat{R}\partial_t\hat{R}^{\dagger} = \hat{H}^{\mathrm{R}}_0 + \hat{H}^{\mathrm{R}}_{\mathrm{drv}}, \tag{3}$$

where

$$\hat{H}^{\mathrm{R}}_0 = -\mu\sum_{i=1}^{L}\hat{n}_i - J\sum_{i=1}^{L-1}(\hat{a}_i^{\dagger}\hat{a}_{i+1} + \mathrm{H.c.}) + \frac{U}{2}\sum_{i=1}^{L}\hat{n}_i(\hat{n}_i - 1) + V\sum_{i=1}^{L-1}\hat{n}_i\hat{n}_{i+1}, \tag{4}$$

$$\hat{H}^{\mathrm{R}}_{\mathrm{drv}} = \Omega\sum_{i=1}^{L-1}(\hat{a}_i\hat{a}_{i+1} + \mathrm{H.c.}), \tag{5}$$

and $\mu = \omega_d - \omega_r$ is the detuning. In the following discussion, we analyze the properties of $\hat{H}^{R}_{\mathrm{tot}}$ both when $\Omega = 0$ and $\Omega > 0$. The driven-dissipative dynamics is governed by the master equation

$$\frac{\partial}{\partial t}\hat{\rho} = -i\big[\hat{H}^{\mathrm{R}}_{\mathrm{tot}}, \hat{\rho}\big] - \frac{\gamma}{2}\sum_{i=1}^{L}(\{\hat{n}_i, \hat{\rho}\} - 2\hat{a}_i\hat{\rho}\hat{a}_i^{\dagger}), \tag{6}$$

where γ is the dissipation rate, and ρ is the density matrix of the system.

We study the quantum phase via hidden order defined by a nonvanishing string order (SO)

$$\mathcal{O}_{\mathrm{S}} = \lim_{|i-j|\to\infty}\left|\left\langle \delta\hat{n}_i e^{i\pi\sum_{k=i+1}^{j-1}\delta\hat{n}_k}\delta\hat{n}_j\right\rangle\right| > 0, \tag{7}$$

and a vanishing density-wave order (DWO)

$$\mathcal{O}_{\mathrm{DW}} = \lim_{|i-j|\to\infty}|\langle\delta\hat{n}_i\delta\hat{n}_j\rangle| = 0, \tag{8}$$

where $\delta\hat{n}_i = \hat{n}_i - \bar{n}$ is the number fluctuation at site i and $\bar{n} = \sum_{i=1}^{L}\langle\hat{n}_i\rangle/L$ is the filling factor [37]. The vanishing DWO implies that quantum fluctuations between two distant sizes are uncorrelated. Yet the nonvanishing SO implies that these fluctuations exhibit a certain infinitely-long-range structure which is "hidden" from DWO. Note that the string order operator is not Hermitian, so SO is not a correlation function. This hidden order is used to characterize the topological Haldane phase with unit filling in the equilibrium context; see Appendix A for more details. Nonequilibrium quench dynamics and thermalization of SO in the context of the spin-chain system have been studied in Refs. [46,47], where the authors assume that the starting state already has SO. In contrast, here we show in Sec. IV that SO can be generated from the vacuum in the driven-dissipative scenario.

III. SYMMETRY OF TWO-PHOTON PARAMETRIC PROCESS

In this section, we analyze the symmetry of the two-photon parametric process by mapping the bosonic system to a spin-chain system. We then analytically and numerically show that the SO of the Haldane phase is robust against weak parametric driving.

We first examine the energy spectrum of the EBH model in the context of the coupled resonator array, ignoring dissipation. The EBH model conserves the number particles, so the excited states can be grouped into manifolds labeled by the total number of particles N, which is an eigenvalue of $\sum_i \hat{n}_i$. Since we work in a regime far from the ultrastrong-coupling regime, i.e., $\omega_r \gg J, U, V$, the ground state of the undriven system is the vacuum; see Fig. 1(b). It has been shown that, at appropriate parameter regimes, the lowest-energy state in the unit-filled manifold ($N = L$) shows the topological Haldane insulator (HI) phase, exhibiting the hidden order [37–39]. We label the many-body state in this phase as $|\mathrm{HI}\rangle$.

As shown below, the detuning μ can be chosen such that $|\mathrm{HI}\rangle$ becomes a gapped ground state of $\hat{H}^{\mathrm{R}}_0$; see Fig. 1(c). We consider a weak drive $\Omega < U, V, J$ such that the filling factor of $|\mathrm{HI}\rangle$ is approximately unaffected by the drive due to the gap. We numerically confirm below that this approximation is valid. We then map the bosonic system onto a spin-1 chain model by only keeping states with site occupation of up to two photons. This is justified by the large on-site interaction $U \gg J$ required for the insulating phases. As a result, the bosonic Fock states $\{|0\rangle_f, |1\rangle_f, |2\rangle_f\}$ can replaced by the spin-1 states $\{|+\rangle_s, |0\rangle_s, |-\rangle_s\}$. The bosonic operators can be replaced with spin-1 operators, i.e., $\hat{a}_i \to \hat{S}_i^{+}/\sqrt{2}$ and $\hat{n}_i \to \hat{\mathbb{1}} - \hat{S}_j^{z}$. In the spin-chain picture, the total bosonic Hamiltonian $\hat{H}^{\mathrm{R}}_{\mathrm{tot}}$ becomes

$$\hat{H}^{S}_{\mathrm{tot,par}} = \sum_{i=1}^{L-1}\big[(J+\Omega)\hat{S}_i^{x}\hat{S}_{i+1}^{x} + (J-\Omega)\hat{S}_i^{y}\hat{S}_{i+1}^{y}\big] + V\sum_{i=1}^{L-1}\hat{S}_i^{z}\hat{S}_{i+1}^{z} + \frac{U}{2}\sum_{i=1}^{L}\big(\hat{S}_i^{z}\big)^2. \tag{9}$$

An additional term $(-\mu + U/2 + V)\sum_i \hat{S}_i^{z}$ has been dropped because it is approximately zero since we assume that the ground state of the undriven system has unit filling and the drive is weak. The system has global $D_2 = Z_2 \times Z_2$ symmetry, i.e., a π rotation of all spins about the X, Y, and Z axes. One can see that the presence of the weak parametric process does not alter this symmetry.

To understand how symmetry-breaking perturbations affect the HI state using a mean-field approximation, let us consider the unitary transformation [40]

$$\hat{U}_{KT} = \prod_{i<j}\exp\big(i\pi\hat{S}_i^{z}\hat{S}_j^{x}\big). \tag{10}$$

This transformation is defined such that the nonlocal SO will be transformed into local order so that the mean-field approximation can be applied. The transformed Hamiltonian is

$$\hat{U}_{KT}\hat{H}^{S}_{\mathrm{tot,par}}\hat{U}_{KT}^{-1} = -(J-\Omega)\sum_{i=1}^{L-1}\hat{S}_i^{y}\exp\big[i\pi\big(\hat{S}_i^{z} + \hat{S}_{i+1}^{x}\big)\big]\hat{S}_{i+1}^{y} - (J+\Omega)\sum_{i=1}^{L-1}\hat{S}_i^{x}\hat{S}_{i+1}^{x} - V\sum_{i=1}^{L-1}\hat{S}_i^{z}\hat{S}_{i+1}^{z} + \frac{U}{2}\sum_{i=1}^{L}\big(\hat{S}_i^{z}\big)^2. \tag{11}$$

We see that this Hamiltonian still involves only nearest-neighbor terms even though the transformation is nonlocal. This is due to the global D_2 symmetry of the Hamiltonian. Local terms that break the global D_2 symmetry will be transformed into nonlocal terms in this picture. As shown in Ref. [40], the motivation for using $\hat{U}_{KT}$ is that SO in the original picture will be transformed into ferromagnetic order (FMO), i.e.,

$$\hat{U}_{KT}\left(\hat{S}_i^z e^{i\pi\sum_{k=i+1}^{j-1}\hat{S}_k^z}\hat{S}_j^z\right)\hat{U}_{KT}^{-1} = \hat{S}_i^z\hat{S}_j^z. \tag{12}$$

Below we show that FMO is stable against weak parametric driving by using a simple mean-field analysis as in Ref. [40], which is then backed up quantitatively by density matrix renormalization group (DMRG) calculations [48].

The mean-field energy is defined as $E_{\rm MF} \equiv \langle\Phi|\hat{U}_{KT}\hat{H}^S_{\rm tot,}\hat{U}_{KT}^{-1}|\Phi\rangle$, where $|\Phi\rangle = \otimes_i A_i|\phi\rangle_i$ is a homogenous product state ansatz, $|\phi\rangle_i = a|0\rangle_i + b|+\rangle_i + c|-\rangle_i$ is a local state, $A_i = (|a|^2+|b|^2+|c|^2)^{-1/2}$ is a normalization factor, and a, b, c are complex numbers. The mean-field energy takes the form

$$\begin{aligned} E_{\rm MF} = \{|a|^2+|b|^2+|c|^2\}^{-2}\Bigg[&\left(\frac{U}{2}-V\right)(|b|^4+|c|^4) \\ &+2\left(\frac{U}{2}+V\right)|b|^2|c|^2 + \left(\frac{U}{2}-2J\right)|a|^2(|b|^2+|c|^2) \\ &-\mathrm{Re}\{2Ja^2(b^{*2}+c^{*2})+4\Omega|a|^2b(c+c^*)\}\Bigg], \end{aligned} \tag{13}$$

where $*$ indicates a complex conjugate. $E_{\rm MF}$ is minimized when the last two terms inside Re{...} are maximized. This happens when when a, b, and c are real. Without loss of generality, we can set $a = 1$ and get

$$\begin{aligned} E_{\rm MF} = \{1+b^2+c^2\}^{-2}\Bigg[&\left(\frac{U}{2}-V\right)(b^4+c^4) \\ &+2\left(\frac{U}{2}+V\right)b^2c^2 + \left(\frac{U}{2}-4J\right)(b^2+c^2) - 8\Omega bc\Bigg]. \end{aligned} \tag{14}$$

The mean-field energy landscape is shown in Fig. 2 with $U = 5J$ and $V = 2.8J$. When $\Omega = 0$, $E_{\rm MF}$ displays four degenerate FM ground states. This reflects the global D_2 symmetry of the corresponding HI phase because the global D_2 symmetry implies that the state is invariant under the global π rotation about x, y, z axes. Nevertheless, π rotation around the x and y axes also implies π rotation around the z axis. Hence the degeneracy is fourfold. With weak parametric drive $\Omega = 0.1J$, the FM ground states remain fourfold degenerate, confirming that the D_2 symmetry is unbroken.

To corroborate the mean-field picture quantitatively we performed DMRG calculations on the bosonic Hamiltonian $\hat{H}^{\rm R}_{\rm tot}$ in the rotating frame. The degenerate ground states of the HI phase are lifted by forcing the edge sites to have no photon at one end and two photons at another end. The HI state was found as the ground state of $\hat{H}^{\rm R}_0$ by numerically scanning μ. When $\Omega > 0$, the SO and the DWO of the ground state for different Ω are shown in Fig. 3. It confirms that the HI phase is stable against weak parametric driving.

We note that the D_2 symmetry and the mean-field analysis discussed here are based on the effective spin system with

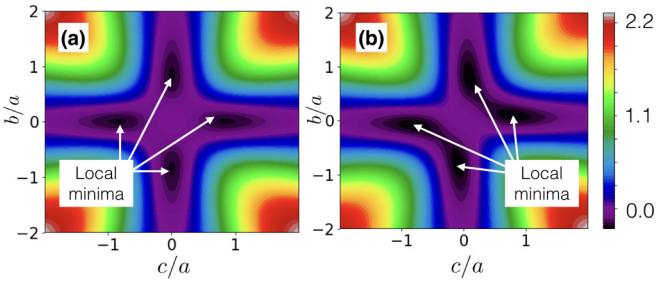

FIG. 2. Mean-field energy landscape E_{MF} plotted against b/a and c/a with $V = 2.8J$ and $U = 5J$. (a) In the absence of drive $\Omega = 0$, the variational ferromagnetic ground state has fourfold ground-state degeneracy, reflecting the global D_2 symmetry of the HI phase. (b) With a weak parametric drive $\Omega = 0.1J$, the ground states remain fourfold degenerate. Hence the symmetry is unbroken.

$\langle\sum_i \hat{S}_i^z\rangle = 0$. The latter is equivalent to having a fixed number of photons in the bosonic picture. This approximation is valid for a weak drive, $\Omega \ll \Delta E$, since the undriven system, in the rotating frame, has a ground state, with the gap ΔE. However, when the drive's amplitude is comparable to ΔE, the driving term will break the conservation of the total number of photons causing $\langle\sum_i \hat{S}_i^z\rangle \neq 0$ in the spin picture. The latter breaks the D_2 symmetry and is not captured in the mean-field analysis shown in Fig. 2.

IV. THE EMERGENCE OF HIDDEN ORDER

In this section, we turn into the driven-dissipative scenario far from equilibrium which involves photon loss. The dynamics of the system is now described by the Lindblad master equation (6). Time evolution is obtained by solving the

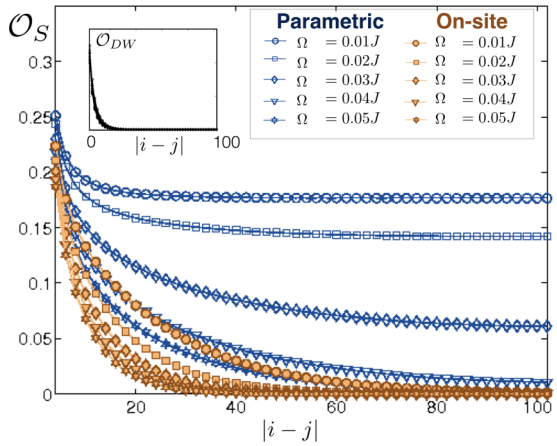

FIG. 3. DMRG calculations of SO and DWO of the ground state of $\hat{H}^{\rm R}_{\rm tot}$ with $\mu = 7.5J$, $U = 5J$, and $V = 3.3J$. It shows that weak parametric drives preserve the HI phase, which is characterized by a nonvanishing SO and a vanishing DWO. Both SO and DWO are zero when on-site drives are used, indicating that the HI phase is destroyed. The DMRG calculations were performed with open boundary conditions and the bond dimension of 200. The system's size is $L = 300$. The local Hilbert space in the numerics is truncated at the four-photon Fock state ($\Delta E^R_{\rm HI} = \langle{\rm HI}|\hat{H}^R_0|{\rm HI}\rangle \approx -1.22LJ$ and $\Delta E^L_{\rm HI} = \langle{\rm HI}|\hat{H}_0|{\rm HI}\rangle \approx 6.28LJ$).

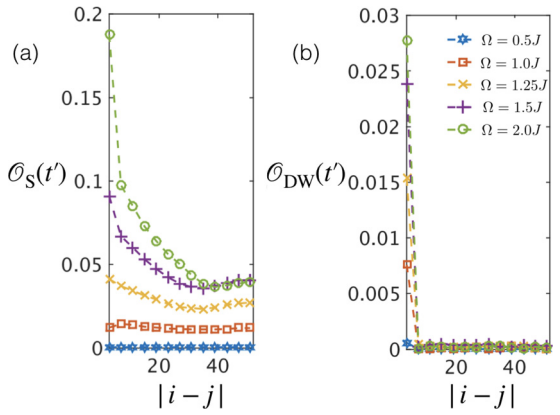

FIG. 4. Hidden order at a transient time during the driven-dissipative dynamics. Time evolution of the system ($L = 100$) evolving under Eq. (6) with parametric drive, obtained by using the quantum trajectories with 200 trajectories and the TEBD algorithm with the bond dimension of 100. (a) SO and (b) DWO measured at the time $t' = 0.25/J$ as a function of $|i - j|$ for different driving amplitudes $\Omega/J = 0.5, 1.0, 1.25, 1.5, 2.0$.

Lindblad master equation by using the quantum trajectories [49] and the time-evolving block decimation (TEBD) algorithm [50]. We start from the vacuum and switch on suddenly the parametric drive.

In Fig. 4, we plot SO and DWO measured at the time $t' = 0.25/J$ as a function of $|i - j|$ for different driving amplitudes $\Omega/J = 0.5$, 1.0, 1.25, 1.5, 2.0. The parameters are chosen such that the lowest-energy state in the unit-filled manifold of $\hat{H}_0$ is in the Haldane state $|\mathrm{HI}\rangle$. The frequency ω_d is chosen to be resonant with the transition between the vacuum state and $|\mathrm{HI}\rangle$, i.e., $\omega_d = \Delta E^L_{\mathrm{HI}}/L$. Note that this frequency is different than the one used in the previous section. It can be seen that, at this time, the SO is finite and increases with the driving amplitude Ω, while DWO remains zero.

In Figs. 5(a)–5(c), we plot the filling factor, OS, and DWO as a function of time. We observe the hidden order in the transient dynamics emerging from the vacuum but eventually dying out at the steady state. We observe that the maximum value of the hidden order is increased with the amplitude of the drive, as also seen in Fig. 4. However, the duration that the hidden order exists is reduced for a stronger drive. This regime corresponds to the regime where OS > DWO > 0 [40]. We found that the optimal value of the driving amplitude is around $1.25J$–$1.5J$, where the maximum OS is ∼0.05 and the existence duration is $\sim 1/\Omega$.

We found that, when OS is at maximum, the overlap $\mathrm{Tr}(\hat{\rho}(t)|\mathrm{HI}\rangle\langle\mathrm{HI}|)$ is on the order of 10^{-3}. This small overlap implies that the system is far from the equilibrium Haldane state. This is expected because the latter is defined for an insulating unit-filled state, while here the number of particles is not conserved due the coherent drive and losses. However, the emergence of the string order here is intimately related to the symmetry of the equilibrium Haldane phase. As discussed in the next section, when the parametric drive is replaced by an on-site driving that breaks the symmetry of the equilibrium Haldane phase, the hidden order cannot emerge from the vacuum. Finally, we note that the emergence of the hidden order from the vacuum here does not imply that two distant spins are correlated immediately after the quench, since DWO = 0 at $Jt \ll 1$. At the steady state, although the hidden order vanishes, we found a weak DWO of order $\sim 10^{-3}$–10^{-4}.

In Figs. 5(d)–5(f) we study the effect of photon loss. For the parameter regime given in the caption of Figs. 5(d)–5(f), we find that, without loss, OS reaches its maximum of OS ∼ 0.1 at $Jt \sim 2$. The maximum OS is reduced to 0.05 when $\gamma = 0.05J$ and continues to decrease as γ is increased. The rapid reduction of OS when γ is nonzero comes from the fact that a single photon loss can destroy OS since it breaks the symmetry and becomes nonlocal in the transformed picture discussed in Sec III. At $Jt = 2$, there are about $\bar{n}L \sim 50$ photons in the system. Hence the decay rate is $\sim 50\gamma = 2.5J$, which is comparable to the hopping rate.

In Figs. 5(e)–5(i), we study the effect of the V term. We found that, when $V = 0$, a transient SO order still exists.

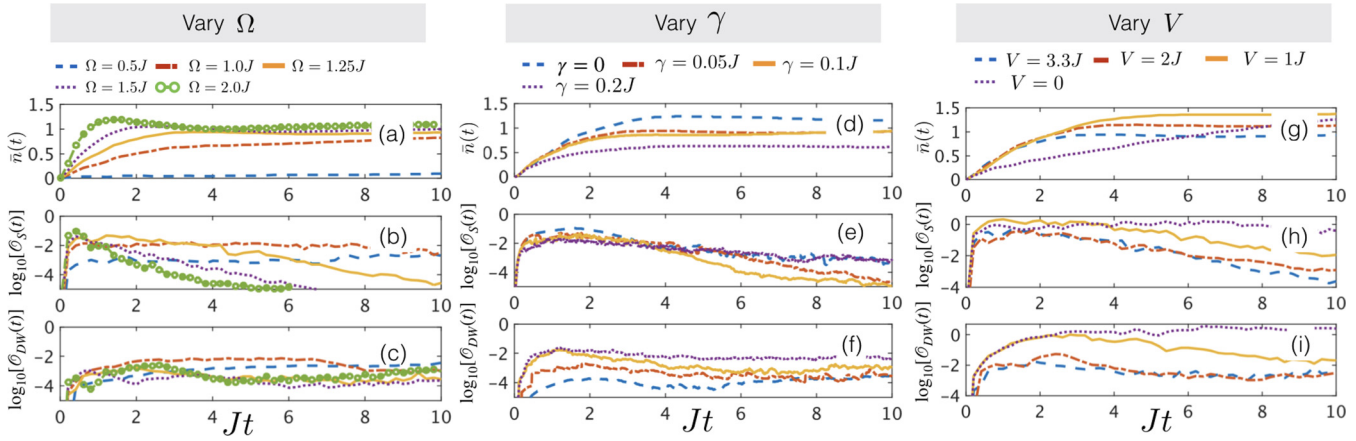

FIG. 5. Rise and fall of the hidden order in the driven-dissipative dynamics. Time evolution of the system ($L = 50$) evolving under Eq. (6) with parametric drive, obtained by using the quantum trajectories with 100 trajectories and the TEBD algorithm with the bond dimension of 100. In panels (a)–(c), we vary the amplitude of the drive with $\mu = 6.28J$, $U = 5J$, $V = 3.3J$, and $\gamma = 0.05J$. In panels (d)–(f), we vary the photon loss rate with $\mu = 6.28J$, $U = 5J$, $V = 3.3J$, and $\Omega = 1.25J$. In panels (g)–(i), we vary V with $\mu = 6.28J$, $U = 5J$, $\gamma = 0.05J$, and $\Omega = 1.25J$.

However, in the same regime we observe a large transient DWO whose magnitude is larger than SO. This implies that there is no hidden order during the evolution [40]. As V is increased, this DWO is strongly suppressed while the SO remains appreciable leading to the transient hidden order.

V. COMPARISON WITH ON-SITE COHERENT DRIVE

Although the nearest-neighbor parametric driving discussed so far has been experimentally realized [43], it is not a common drive used in quantum optics. Previous literature instead considers a more conventional one-photon drive [14–17,19–22]:

$$\hat{H}_{\text{local}} = \Omega \sum_{i=1}^{L} (\hat{a}_i e^{i\omega_d t} + \hat{a}_i^\dagger e^{-i\omega_d t}). \tag{15}$$

In this section we show that this drive has a different symmetry than the two-photon drive discussed in the previous section. To see this, let us consider the rotating frame defined by $\hat{R}$ as before. In this frame the drive becomes

$$\hat{H}^{\text{R}}_{\text{local}} = -\omega_p \sum_{i}^{L} \hat{n}_i + \Omega \sum_{i=1}^{L} (\hat{a}_i + \hat{a}_i^\dagger). \tag{16}$$

Assuming a weak drive and mapping the system to a spin-chain system, the total Hamiltonian becomes

$$\hat{H}^{S}_{\text{tot,loc}} = \sum_{i=1}^{L-1} \left(J\hat{S}_i^x \hat{S}_{i+1}^x + J\hat{S}_i^y \hat{S}_{i+1}^y + V\hat{S}_i^z \hat{S}_{i+1}^z \right) + \sum_{i=1}^{L} \left[\frac{U}{2} \left(\hat{S}_i^z\right)^2 + \Omega \hat{S}_i^x \right]. \tag{17}$$

Again the term $\sum_i \hat{S}_i^z$ is dropped due to the unit-filling condition. We can see that the term $\Omega\hat{S}_i^x$ is not invariant under the transformation $\hat{S}_i^x \to -\hat{S}_i^x$. Hence it breaks the global D_2 symmetry. When applying the nonlocal unitary transformation $\hat{U}_{\text{KT}}$, the terms becomes

$$\hat{U}_{\text{KT}} \left(\sum_{i=1}^{L} \hat{S}_i^x \right) \hat{U}_{\text{KT}}^{-1} = \sum_{i=1}^{L} \hat{S}_i^x \exp\left(i\pi \sum_{k=i+1}^{L} \hat{S}_k^x \right), \tag{18}$$

which is highly nonlocal. Hence the FM phase in the transformed picture will be destroyed even for a weak drive. In the original picture, this means that $|\text{HI}\rangle$ and its string order is destroyed in the presence of the on-site drive. This is confirmed by DMRG calculations, shown in Fig. 3. When performing the time evolution including dissipation using TEBD calculations, we also found that the SO remains zero throughout the time evolution.

VI. CONCLUSION

We have shown that the dynamics of quantum many-body systems driven by parametric processes can exhibit hidden order which goes beyond local order parameters. The hidden order can arise in a transient case even when symmetry-breaking dissipation is included. We show that this drive respects the symmetry of the HI phase while the conventional on-site drive does not. Our work opens a new direction to explore the role of the nonlocal order and symmetry in nonequilibrium settings as well as its connection to the equilibrium SPT phases.

ACKNOWLEDGMENTS

The authors acknowledge fruitful discussions with P. Nang Ma. The authors gratefully acknowledge financial support through the National Research Foundation and Ministry of Education Singapore (partly through the Tier 3 Grant "Random numbers from quantum processes"). The research leading to these results has received funding from the European Research Council under the European Union's Seventh Framework Programme (FP7/2007-2013) Grant Agreement No. 319286 Q-MAC, UK EPSRC funding Grant No. EP/K038311/1, EPSRC under Grants No. EP/P025110/1, No. EP/P009565/1, and No. EP/P01058X/1. The Polisimulator project was co-financed by Greece and the EU Regional Development Fund.

APPENDIX A: THE HIDDEN ORDER

The hidden order was first introduced as a nonlocal order parameter to differentiate the Haldane spin-1 dfphase from other topologically trivial spin phases [51]. This later motivated the notion of SPT phases, which lie outside the conventional paradigm of Landau's symmetry-breaking theory and so cannot be identified by a local order parameter [26]. The hidden order was then generalized to the bosonic system by Ref. [37]. This bosonic hidden order was originally used to identify ground-state phases of the EBH model with unit filling $\bar{n} = 1$ [37–39]. It distinguishes the topological Haldane insulator (HI) phase ($\mathcal{O}_{\text{S}} > 0$, $\mathcal{O}_{\text{DW}} = 0$) from other topologically trivial insulating phases which are the Mott phase ($\mathcal{O}_{\text{S}} = \mathcal{O}_{\text{DW}} = 0$) and the density-wave phase ($\mathcal{O}_{\text{DW}} > \mathcal{O}_{\text{S}} > 0$). The model also exhibits a superfluid phase when the interactions U and V are much smaller than the hopping strength J.

To visualize the structure of this hidden order, it is helpful to map the bosonic system to its equivalent spin-1 chain model with the total magnetization along the Z axis fixed to zero [37]. This is done by truncating the bosonic Hilbert space up to $n = 0$ photons per site. This is justified by the large on-site interaction $U \gg J$ required for the insulating phases. As a result, the bosonic Fock states $\{|0\rangle_f, |1\rangle_f, |2\rangle_f\}$ can be replaced by the spin-1 states $\{|+\rangle_s, |0\rangle_s, |-\rangle_s\}$, i.e.,

$$|0\rangle_f \to |+\rangle_s, \quad |1\rangle_f \to |0\rangle_s, \text{ and } |2\rangle_f \to |-\rangle_s. \tag{A1}$$

In this picture, the Mott insulator $|1111\cdots\rangle_f$ and the density wave,$|2020\cdots\rangle_f$ become the ferromagnetic phase $|0000\cdots\rangle_s$ and the antiferromagnetic phase $|-+-+\cdots\rangle_s$, respectively. The HI phase becomes the phase similar to the antiferromagnetic phase but with an arbitrary number of $|0\rangle_s$ between the states $|+\rangle_s$ and $|-\rangle_s$, e.g., $|+00-0+0000-\cdots\rangle_s$ [40,41,52]. Since the number of $|0\rangle_s$ between two spins is random, the two spins are uncorrelated, i.e., $\mathcal{O}_{\text{DW}} = 0$. However, the alternating long-range pattern between $|+\rangle_s$ and $|-\rangle_s$ is picked up by SO.

To understand the symmetry of the system, let us replace the bosonic operators with spin-one operators, i.e., $\hat{a}_i \to \hat{S}_i^+/\sqrt{2}$ and $\hat{n}_i \to \hat{\mathbb{1}} - \hat{S}_j^z$. The extended Bose–Hubbard model with the unit filling is then mapped to the effective spin

Hamiltonian,

$$\hat{H}_0^S = J\sum_{i=1}^{L-1}\left(\hat{S}_i^x\hat{S}_{i+1}^x + \hat{S}_i^y\hat{S}_{i+1}^y\right) + V\sum_{i=1}^{L-1}\hat{S}_i^z\hat{S}_{i+1}^z + \frac{U}{2}\sum_{i=1}^{L}\left(\hat{S}_i^z\right)^2. \tag{A2}$$

The term $\sum_i \hat{S}_i^z$ is dropped because it is zero for the unit-filled state. Similar to the EBH model, this model has gapped ground-state phases including all spin phases mentioned above [40,41]. It has the global $D_2 = Z_2 \times Z_2$ symmetry, i.e., π rotation of all spins about the X, Y, and Z axes. The Haldane phase is a SPT phase protected by this symmetry, meaning that its edge states are robust against any perturbations that are smaller that the excitation gap and do not break the symmetry.

APPENDIX B: IMPLEMENTATION OF PARAMETRIC PUMPING USING CIRCUIT QED

In this section, we propose an implementation of the Bose–Hubbard model driven by parametric pumping, using circuit-QED architecture. The cross-Kerr nonlinearity term Vn_in_j has already been discussed in the literature [19,53] and can be integrated into our circuit, so we do not reproduce it here. Note that this term has also been implemented experimentally for a dimer [53]. Nevertheless, circuit designs discussed in Refs. [19,53] do lead to extra terms in the Hamiltonian that needed further investigation.

Our circuit diagram is shown in Fig. 6. The flux variable is defined as $\phi_i = -\int V_i dt$, where V_i is a voltage at the corresponding position. As will be shown below, this quantity can be quantized to the form $\phi_i = \alpha(a_i + a_i^\dagger)$, where a_i, $a_i^\dagger$ are bosonic operators of an "artificial" photon at site i and α is some constant that depends on the circuit's elements. We first describe the rules of Josephson junctions which introduce various kinds of nonlinearities to the system and then explicitly show how to quantize the circuit.

The first Josephson junction $E_{J,U}$ (labeled in orange in Fig. 6) corresponds to a $\chi^{(3)}$ nonlinear material, which gives rise to the on-site Kerr nonlinearity $\frac{U}{2}n_i(n_i-1)$. The junction is biased by the magnetic flux $\Phi_g = \pi\phi_0$, where $\phi_0 = \hbar/2e$, and shunted by a small inductor L' to produce a repulsive interaction $U > 0$. The second Josephson junction E_{J,Ω_p} (labeled in yellow in Fig. 6) corresponds to a $\chi^{(2)}$ nonlinear material, which is responsible for a parametric-down-conversion (PDC) process. The PDC process converts a pumped photon with frequency $2\omega_p$ into a pair of photons with frequency ω_p. Here the pumped photons come from an oscillating flux bias $\Phi_b(t) = \pi\phi_0/2 + \phi_b(t)$.

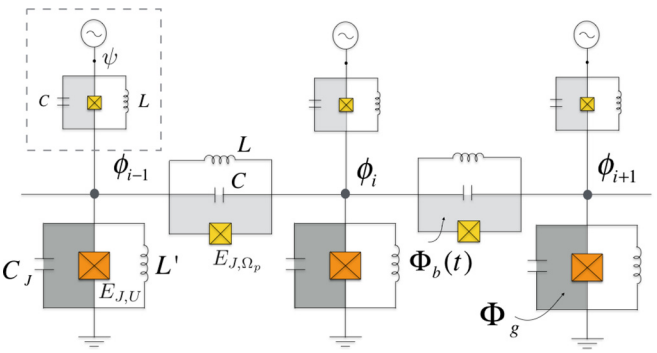

FIG. 6. Proposed circuit diagram that implements the Bose–Hubbard model and parametric driving.

As discussed in Ref. [18], this PDC process leads to both nearest-neighbor parametric pumping of the form $(a_i^\dagger a_{i+1}^\dagger +$ H.c.) and on-site parametric pumping of the form $(a_i^{\dagger 2} + a_i^2)$. The latter can be eliminated by introducing an extra on-site PDC process (labeled in a dotted box in Fig. 6). This extra component is driven by a coherent voltage source ψ, whose phase differs from that of $\phi_b(t)$ by π.

We now show how to quantize the circuit by following the standard procedure [54]. We first write down the circuit's Lagrangian as $\mathcal{L} = \sum_i(\mathcal{L}_i^{\text{on-site}} + \mathcal{L}_i^{\text{hopping}} + \mathcal{L}_i^{pump} + \mathcal{L}_i^{\text{onsite-PDC}})$ where

$$\mathcal{L}_i^{\text{on-site}} = \frac{1}{2}C_J\dot{\phi}_i^2 - \frac{1}{2L'}\phi_i^2 + E_{J,U}\cos\left(\frac{\phi_i + \pi\phi_0}{\phi_0}\right), \tag{B1}$$

$$\mathcal{L}_i^{\text{hopping}} = \frac{1}{2}C(\dot{\phi}_i - \dot{\phi}_{i+1})^2 - \frac{1}{2L}(\phi_i - \phi_{i+1})^2, \tag{B2}$$

$$\mathcal{L}_i^{\text{pump}} = E_{J,\Omega_p}\cos\left(\frac{\phi_i - \phi_{i+1} + \pi\phi_0/2 + \phi_b(t)}{\phi_0}\right), \tag{B3}$$

$$\mathcal{L}^{\text{onsite-PDC}} = \frac{1}{2}C(\dot{\phi}_i - \dot{\psi})^2 + E_{J,\Omega_p}\cos\left(\frac{\phi_i - \psi + \pi\phi_0/2}{\phi_0}\right). \tag{B4}$$

Assuming $C/(C_J + 3C) \ll 1$, the Hamiltonian can then be obtained by using the Legendre transformation [55]. A conjugate momentum of ϕ_i is defined as $q_i = \sqrt{3C + C_J}\partial\mathcal{L}/\partial\dot{\phi}_i$. Both ϕ_i and q_i are then quantized by defining ladder operators a_i, $a_i^\dagger$ according to $\phi_i = (\tilde{L}/4\tilde{C})^{1/4}(a_i + a_i^\dagger)$ and $q_i = i(\tilde{C}/4\tilde{L})^{1/4}(-a_i + a_i^\dagger)$, where $\tilde{C} = C_J + 3C$ and $\tilde{L} = [1/L' + 3/L - E_{J,U}/\phi_0^2]^{-1}$ are effective capacitance and effective inductance, respectively. It follows that $[a_i, a_j^\dagger] = \delta_{ij}$. In addition, after the Legendre transformation, the quadratic terms in $\mathcal{L}$ are transformed into $\sum_i \omega_c a_i^\dagger a_i$, where $\omega_c = 1/\sqrt{\tilde{L}\tilde{C}}$ is a frequency of the artificial photon. We can see that, by adding a small shunting inductor L', ω_c is guaranteed to be real.

To see the emergence of the on-site Kerr nonlinearity U and PDC, we first notice that the Legendre transformation only introduces a minus sign to the "potential" terms, including all the cosine terms in $\mathcal{L}$. Hence, the onsite Kerr nonlinearity can be seen by expanding the cosine function in Eq. (B1), taking into account the normal ordering as [56]

$$E_{J,U}\cos[\lambda(a_i + a_i^\dagger)] = E_{J,U}e^{-\lambda^2/2}\left(1 - \lambda^2 a_i^\dagger a_i + \frac{\lambda^4}{4}a_i^\dagger a_i^\dagger a_i a_i + \cdots\right),$$

where $\lambda = (2E_{\tilde{C}}/E_{\tilde{L}})^{1/4}$, with $E_{\tilde{C}} = e^2/2\tilde{C}$ and $E_{\tilde{L}} = \phi_0^2/\tilde{L}$. For a large $E_{\tilde{L}}/E_{\tilde{C}}$, we can neglect the terms that are higher than forth order [57].

The parametric pumping term comes directly from the sine expansion in Eq. (B3). For illustrative purpose, we neglect the normal-ordering and consider the sine expansion up to the third order as

$$E_{J,\Omega_p}\sin\left(\frac{\phi_i-\phi_{i+1}+\phi_b}{\phi_0}\right) \approx \frac{E_{J,\Omega_p}}{\phi_0}(\phi_i-\phi_{i+1})-\frac{E_{J,\Omega_p}}{3!\phi_0^3}(\phi_i-\phi_{i+1}+\phi_b)^3,$$

where we neglect the term $E_{JJ}\phi_b/\phi_0$, since it does not act on the system. The linear term can also be eliminated by applying a current bias I at both ends of the array. After applying the rotating wave approximation, the only third-order terms that survive are of the form $(b^\dagger a_i a_{i+1}+\text{H.c.})$ and $(b^\dagger a_i^2+b^\dagger a_{i+1}^2+\text{H.c.})$, where $b^\dagger$ is a creator of the field ϕ_b. The latter is canceled by the onsite PDC process in Eq. (B4).

Finally by explicitly writing down the time dependence of b and $b^\dagger$ and replacing them with c numbers, the Hamiltonian can be cast into the form

$$\mathcal{H}=\sum_i(\omega+\delta\omega)a_i^\dagger a_i+\frac{U}{2}a_i^\dagger a_i^\dagger a_i a_i-J(a_i^\dagger a_{i+1}+\text{H.c.}) +\Omega_p(e^{i2\omega_p t}a_i a_{i+1}+\text{H.c.}), \tag{B5}$$

where $\omega=1/\sqrt{\tilde{L}\tilde{C}}$, $\delta\omega=E_J\lambda^2(1-e^{-\lambda^2/2})$, $U/2=E_J\lambda^4e^{-\lambda^2/2}/4$ and $J=\omega/2(\tilde{L}/L-C/\tilde{C})$. The parametric pumping coefficient Ω_p is directly proportional to E_{JJ}. However, its explicit form depends on the relation between ϕ_b and $(b+b^\dagger)$ and hence depends on how ϕ_b is generated.

Our circuit allows the Hamiltonian parameters to be tuned independently: μ can be tuned directly by changing ω_p, U comes from the first Josephson junction $E_{J,U}$, J comes from the coupling LC oscillator, while Ω_p independently comes from the second Josephson junction E_{J,Ω_p}. As an example, $U/J\sim 10$ can be realistically obtained by using $\tilde{L}/L\sim 5\times 10^{-3}$, $\lambda\sim 0.4$, and $E_J/E_C\sim 10^5$ [58,59]. For this setting, we would have a negligible frequency correction $\delta\omega/\omega\sim 0.02$. Note that this value of λ also ensures that it is a good approximation to expand the cosine term in Eq. (B5) up to fourth order, as for the case of a transmon qubit [57].

[1] D. E. Chang, V. Vuletić, and M. D. Lukin, Nat. Photonics **8**, 685 (2014).
[2] C. Noh and D. G. Angelakis, Rep. Prog. Phys. **80**, 016401 (2017).
[3] D. G. Angelakis, *Quantum Simulations with Photons and Polaritons* (Springer International Publishing, Switzerland, 2017).
[4] J. I. Cirac and P. Zoller, Nat. Phys. **8**, 264 (2012).
[5] T. H. Johnson, S. R. Clark, and D. Jaksch, EPJ Quantum Technol. **1**, 10 (2014).
[6] D. G. Angelakis, M. F. Santos, and S. Bose, Phys. Rev. A **76**, 031805(R) (2007).
[7] M. J. Hartmann, F. G. S. L. Brandao, and M. B. Plenio, Nat. Phys. **2**, 849 (2006).
[8] A. D. Greentree, C. Tahan, J. H. Cole, and L. C. L. Hollenberg, Nat. Phys. **2**, 856 (2006).
[9] A. Kay and D. G. Angelakis, Europhys. Lett. **84**, 20001 (2008).
[10] J. Cho, D. G. Angelakis, and S. Bose, Phys. Rev. Lett. **101**, 246809 (2008).
[11] J. Tangpanitanon, V. M. Bastidas, S. Al-Assam, P. Roushan, D. Jaksch, and D. G. Angelakis, Phys. Rev. Lett. **117**, 213603 (2016).
[12] P. Roushan, C. Neill, J. Tangpanitanon, V. M. Bastidas, A. Megrant, R. Barends, Y. Chen, Z. Chen, B. Chiaro, A. Dunsworth *et al.*, Science **358**, 1175 (2017).
[13] V. V. Albert and L. Jiang, Phys. Rev. A **89**, 022118 (2014).
[14] T. Grujic, S. R. Clark, D. Jaksch, and D. G. Angelakis, New J. Phys. **14**, 103025 (2012).
[15] I. Carusotto, D. Gerace, H. E. Türeci, S. De Liberato, C. Ciuti, and A. Imamoğlu, Phys. Rev. Lett. **103**, 033601 (2009).
[16] M. J. Hartmann, Phys. Rev. Lett. **104**, 113601 (2010).
[17] R. O. Umucalilar and I. Carusotto, Phys. Rev. Lett. **108**, 206809 (2012).
[18] C.-E. Bardyn and A. İmamoğlu, Phys. Rev. Lett. **109**, 253606 (2012).
[19] J. Jin, D. Rossini, R. Fazio, M. Leib, and M. J. Hartmann, Phys. Rev. Lett. **110**, 163605 (2013).
[20] T. Grujic, S. R. Clark, D. Jaksch, and D. G. Angelakis, Phys. Rev. A **87**, 053846 (2013).
[21] M. Fitzpatrick, N. M. Sundaresan, A. C. Y. Li, J. Koch, and A. A. Houck, Phys. Rev. X **7**, 011016 (2017).
[22] J. J. Mendoza-Arenas, S. R. Clark, S. Felicetti, G. Romero, E. Solano, D. G. Angelakis, and D. Jaksch, Phys. Rev. A **93**, 023821 (2016).
[23] H. Wilming, M. J. Kastoryano, A. H. Werner, and J. Eisert, J. Math. Phys. **58**, 033302 (2017).
[24] E. M. Kessler, G. Giedke, A. Imamoglu, S. F. Yelin, M. D. Lukin, and J. I. Cirac, Phys. Rev. A **86**, 012116 (2012).
[25] X.-G. Wen, Rev. Mod. Phys. **89**, 041004 (2017).
[26] D. Pérez-García, M. M. Wolf, M. Sanz, F. Verstraete, and J. I. Cirac, Phys. Rev. Lett. **100**, 167202 (2008).
[27] J. Haegeman, D. Pérez-García, I. Cirac, and N. Schuch, Phys. Rev. Lett. **109**, 050402 (2012).
[28] M. Z. Hasan and C. L. Kane, Rev. Mod. Phys. **82**, 3045 (2010).
[29] X.-L. Qi and S.-C. Zhang, Rev. Mod. Phys. **83**, 1057 (2011).
[30] Z.-C. Gu and X.-G. Wen, Phys. Rev. B **80**, 155131 (2009).
[31] X. Chen, Z.-C. Gu, and X.-G. Wen, Phys. Rev. B **82**, 155138 (2010).
[32] X. G. Wen, Int. J. Mod. Phys. B **04**, 239 (1990).
[33] C. Nayak, S. H. Simon, A. Stern, M. Freedman, and S. Das Sarma, Rev. Mod. Phys. **80**, 1083 (2008).
[34] N. Goldman, J. C. Budich, and P. Zoller, Nat. Phys. **12**, 639 (2016).
[35] T. Ozawa, H. M. Price, A. Amo, N. Goldman, M. Hafezi, L. Lu, M. C. Rechtsman, D. Schuster, J. Simon, O. Zilberberg *et al.*, Rev. Mod. Phys. **91**, 015006 (2019).

[36] L. Lu, J. D. Joannopoulos, and M. Soljačić, Nat. Photonics **8**, 821 (2014).
[37] E. G. Dalla Torre, E. Berg, and E. Altman, Phys. Rev. Lett. **97**, 260401 (2006).
[38] E. Berg, E. G. Dalla Torre, T. Giamarchi, and E. Altman, Phys. Rev. B **77**, 245119 (2008).
[39] D. Rossini and R. Fazio, New J. Phys. **14**, 065012 (2012).
[40] T. Kennedy and H. Tasaki, Commun. Math. Phys. **147**, 431 (1992).
[41] F. Pollmann, E. Berg, A. M. Turner, and M. Oshikawa, Phys. Rev. B **85**, 075125 (2012).
[42] C. Joshi, F. Nissen, and J. Keeling, Phys. Rev. A **88**, 063835 (2013).
[43] B. Abdo, A. Kamal, and M. Devoret, Phys. Rev. B **87**, 014508 (2013).
[44] F. Verstraete, V. Murg, and J. Cirac, Adv. Phys. **57**, 143 (2008).
[45] S. Al-Assam, S. R. Clark, and D. Jaksch, J. Stat. Mech.: Theory Exp. (2017) 093102.
[46] L. Mazza, D. Rossini, M. Endres, and R. Fazio, Phys. Rev. B **90**, 020301(R) (2014).
[47] M. Calvanese Strinati, L. Mazza, M. Endres, D. Rossini, and R. Fazio, Phys. Rev. B **94**, 024302 (2016).
[48] U. Schollwoeck, Ann. Phys. **96**, 326 (2011).
[49] A. J. Daley, Adv. Phys. **63**, 77 (2014).
[50] G. Vidal, Phys. Rev. Lett. **91**, 147902 (2003).
[51] M. den Nijs and K. Rommelse, Phys. Rev. B **40**, 4709 (1989).
[52] M. Oshikawa, J. Phys.: Condens. Matter **4**, 7469 (1992).
[53] E. T. Holland, B. Vlastakis, R. W. Heeres, M. J. Reagor, U. Vool, Z. Leghtas, L. Frunzio, G. Kirchmair, M. H. Devoret, M. Mirrahimi, and R. J. Schoelkopf, Phys. Rev. Lett. **115**, 180501 (2015).
[54] M. H. Devoret, *Quantum Fluctuations in Electrical Circuits*, edited by S. Reynaud, S. Giacobino, and J. Zinn-Justin, Les Houches Session LXIII, 1995, Quantum Fluctuations (Elsevier Science B.V., 1997), pp. 351–386.
[55] A. Nunnenkamp, J. Koch, and S. M. Girvin, New J. Phys. **13**, 095008 (2011).
[56] M. Leib, F. Deppe, A. Marx, R. Gross, and M. J. Hartmann, New J. Phys. **14**, 075024 (2012).
[57] J. Koch, T. M. Yu, J. Gambetta, A. A. Houck, D. I. Schuster, J. Majer, A. Blais, M. H. Devoret, S. M. Girvin, and R. J. Schoelkopf, Phys. Rev. A **76**, 042319 (2007).
[58] M. H. Devoret and R. J. Schoelkopf, Science **339**, 1169 (2013).
[59] J. Q. You and F. Nori, Phys. Today **58**(11), 42 (2005).